

Article

# Parametric Studies of Effect of Cavitation Jet Modes on Wear Rate of Surface of Structural Materials

Alexey Mednikov, Olga Zilova, Aleksandr Tkhabisimov \*, Marat Dasaev and Sergey Grigoriev

Laboratory of Functional Coatings in Power Engineering, Federal State Budget Educational Institution of Higher Education, MIREA-Russian Technological University, 78 Vernadskogo Ave., Moscow 119454, Russia

\* Correspondence: thabisimov@mirea.ru; Tel.: +7-917-555-9192

**Abstract:** In this study the kinetic curves of cavitation wear of cast steels 20 GL and 30 L used for production of critical elements of hydraulic machines were obtained. The typical predominance of growth rate of cavitation mark diameter over its depth was found on the surfaces of the investigated cast steels. The revealed phenomenon made it possible to offer a formula for estimating the volume removal of the examined cast steels in order to expand the scope of the method according to ASTM G134-17. This method uses profilometry and microscopy and allows to determine cavitation resistance both for homogeneous and heterogeneous materials, including materials after modification of their surface (with different types of coatings and hardenings).

**Keywords:** hydraulics; cavitation; jet impact; test operation parameters; wear dynamics; volume removal

## 1. Introduction

Damage of working surfaces of hydraulic turbine blades, propellers, impellers, and stator parts of pump equipment is mainly caused by cavitation impact of medium on the functional surfaces of the equipment during the course of complex physical phenomena and processes.

The study of physical causes of occurrence and development of cavitation [1–5], identification of wear patterns [6–13] on the basis of experimental research, and creation of theoretical models for further evaluation of effectiveness of developed and applied protection techniques continue to be urgent tasks.

To date, a large amount of scientific work is related to the study of the emergence and behavior of cavitation bubbles [14–17], as well as the study of the dynamics of destruction of various materials [18–24] and methods of their hardening, as well as various kinds of condensation and diffusion coatings [25–30]. Cobalt, nickel, aluminum and titanium alloys, composites, non-ferrous metals, alloyed and unalloyed steels receive special attention. On the other hand, casting steels such as 20 GL and 30 L, which are widely used in the production of hydraulic components, have been little studied.

The development and further effective use of a structural material or passive method of its protection under cavitation attack is based on the determination of wear patterns using computer models and conducting comprehensive experimental studies [31–35]. The discovery of the patterns of cavitation wear and the determination of wear resistance criteria of materials are engaged by many scientists, using for this purpose various tools of analysis, laboratory, and field experiments [36–39].

The cavitation test rigs and facilities used in laboratory experiments can be divided into three groups: facilities simulating the occurrence of cavitation in conditions close to natural, high-frequency test rigs, and jet test rigs. This study considers the results obtained using the jet cavitation test rig created by authors. Analogues of such test rig are widely used in the world practice [32,35,40–42].

Interpretation and reporting of cavitation erosion test data are made difficult by two factors. The first is that the rate of erosion (material loss) is not constant with time.



**Citation:** Mednikov, A.; Zilova, O.; Tkhabisimov, A.; Dasaev, M.; Grigoriev, S. Parametric Studies of Effect of Cavitation Jet Modes on Wear Rate of Surface of Structural Materials. *Metals* **2023**, *13*, 48. <https://doi.org/10.3390/met13010048>

Academic Editor: Jae Myung Lee

Received: 24 November 2022

Revised: 16 December 2022

Accepted: 20 December 2022

Published: 24 December 2022



**Copyright:** © 2022 by the authors. Licensee MDPI, Basel, Switzerland. This article is an open access article distributed under the terms and conditions of the Creative Commons Attribution (CC BY) license (<https://creativecommons.org/licenses/by/4.0/>).

This makes it impossible to represent the test result fully by a single number, or to predict long-term behavior from a short-term test. The second is that there is no independent or absolute definition of wear resistance, nor can units of measurement be ascribed to it.

Criteria of wear resistance of materials can be essentially varied depending on deformation rate, scale effects, stressed state of surface, influence of medium, etc. All this inevitably makes it difficult to compare the wear resistance according to different criteria with the properties of materials in a sufficiently wide range of changes in their structures and external loading conditions. That is why it is customary to obtain a cavitation wear curve and use it to determine the cavitation resistance of the examined material in the initial state or with a modified surface.

To determine the cavitation resistance, the authors propose a refinement to the method of estimating the volume removal of material, which is calculated using the typical dimensions (diameter and depth) of the cavitation wear spot on the surface, obtained using surface profilometry and microscopy techniques.

This study aims to determine the operating mode of the cavitation jet test rig leading to the maximum cavitation effect on the surface, determine in this mode the wear kinetics of cast steels 20 GL and 30 L with recording the change in depth and diameter of the cavitation wear spot, calculation of the volume removal and wear rate of the examined cast steels. To solve the task, a cavitation jet test rig based on ASTM G134-17 standard [43] is used. According to [43], cavitating liquid jet immersed in water volume, released from nozzle under high pressure, impacts the sample surface in such a way that cavities (cavitation bubbles) inside liquid collapse, causing wear of surface.

## 2. Materials and Methods

The cavitation jet test rig has the characteristics presented in Table 1, has a closed-loop system of process liquid supply and cooling, is equipped with a sample positioning system, and allows photo- and video-filming of the cavitation cloud in the process of jet impact.

**Table 1.** Technical characteristics of the cavitation jet test rig.

No.	Parameter	Value
1	Maximum pressure at nozzle exit ( $P_{in}$ )	20 MPa
2	Distance from nozzle to sample surface ( $H$ )	5–55 mm
3	Pressure in test rig chamber ( $P_{out}$ )	0.1 MPa
4	Number of samples engaged in experiment	1
5	Nozzle diameter ( $d_{nozzle}$ )	0.3–2 mm

Diagram of cavitation jet test rig is shown in Figure 1. Appearance and sketch of the cavitation jet test rig are shown in Figure 2.

The cavitation jet test rig functions are as follows. A pre-treated operating liquid (water), cleared of mechanical impurities, enters a small nozzle of cylindrical shape through a high-pressure tube at liquid pressure up to 20 MPa developed by a plunger pump. After exiting the nozzle, the jet interacts with the experimental sample mounted in its positioning system (see Figure 3) inside the test chamber. The sample is placed in the path of the jet and at a certain distance from the nozzle. The pressure and temperature of the liquid are monitored with manometers and thermometer. A pressure regulator makes it possible to monitor and change the pressure developed by the pump.

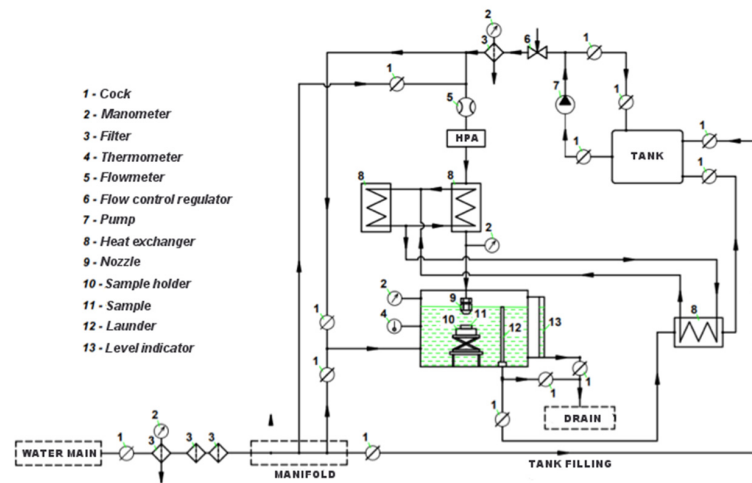


Figure 1. Diagram of prototype cavitation jet test rig.

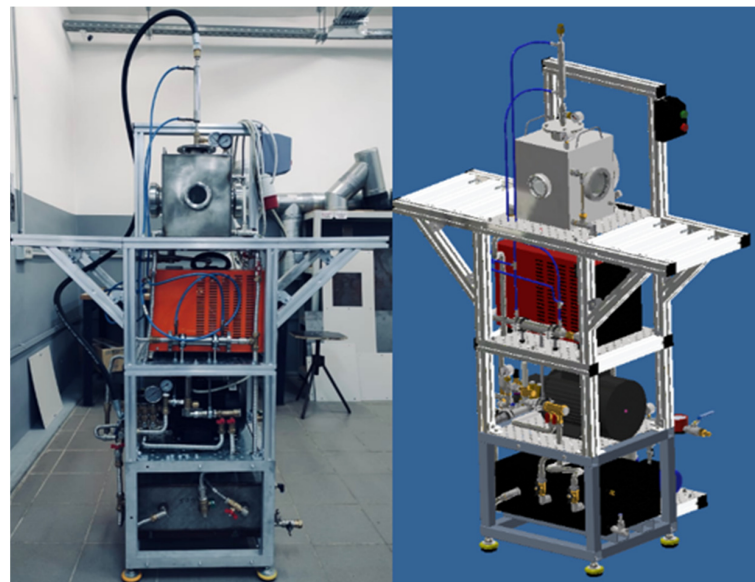


Figure 2. Appearance and sketch of cavitation jet test rig.

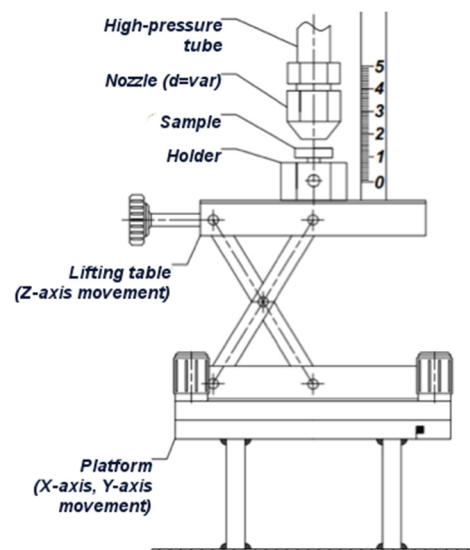


Figure 3. Diagram of sample positioning system in chamber of cavitation jet test rig.

During cavitation tests according to [43], in addition to the inlet pressure ( $P_{in}$ ), pressure in the test rig chamber ( $P_{out}$ ) and nozzle diameter ( $d_{nozzle}$ ), the following parameters are measured:

- Distance from nozzle end to sample surface ( $H$ , mm);
- Mass loss of sample ( $\Delta m_i$ , g);
- Testing time ( $t$ , min).

The mass loss of the sample is calculated using the formula:

$$\Delta m_i = m_o - m_i, \quad (1)$$

where  $m_o$  is the original mass of sample [g];  $m_i$  is the mass of sample after experiment [g];  $i$  is the test number.

We used cylindrical samples with a diameter of 20 mm with a rectangular boss for fixing in the sample holder to perform tests on the cavitation jet test rig.

To determine the optimum distance from the nozzle end to the sample surface, the pressure before the nozzle and the nozzle diameter resulting in the maximum cavitation effect, tests were carried out on coated aluminum specimens with variation of these parameters. Coating is a polymer paint with thickness at 150  $\mu\text{m}$ . The testing time  $t$  was the same for all tests. The chemical composition of aluminum is given in Table 2. The microstructure of uncoated aluminum sample is shown in Figure 4.

**Table 2.** Chemical composition of aluminum.

Fe, %	Si, %	Mn, %	Ti, %	Al, %	Cu, %	Be, %	Mg, %	Zn, %
$\leq 0.3$	$\leq 0.2$	0.4–0.9	$\leq 0.1$	91.8–94.1	3.8–4.3	0.0002–0.005	1.7–2.3	$\leq 0.1$

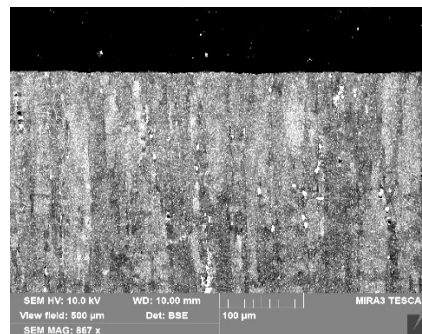


**Figure 4.** Microstructure of uncoated aluminum sample.

After cavitation tests, the surface of coated aluminum samples was examined using a scanning electron microscope and a mechanical stylus profiler. Settings of the SEM microscope are given in Table 3.

**Table 3.** Settings of SEM microscope.

WD	SEM HV	View Field	Det
9–10 mm	10.00 kV	500 $\mu\text{m}$	BSE

The surface condition of samples and the size (diameter— $D_{out}$ ) of cavitation mark were evaluated by surface images obtained using electron microscope, while the depth of cavitation mark  $h$  was determined by profiles obtained using a surface profilometer. Then, the mode that ensured and maximum wear was selected on the basis of the results obtained.

Cavitation tests were conducted on coated aluminum samples at different pressures before nozzle  $P_{in}$ , distances from nozzle to the sample surface  $H$ , and nozzle diameter  $d_{nozzle}$  (see Table 4). Testing time  $t$  was 30 min.

**Table 4.** Conditions of cavitation tests on coated aluminum samples.

Pressure $P_{in}$ , MPa	Nozzle Diameter $d_{nozzle}$ , mm	
	at $H = 5$ mm	at $H = 15$ mm
10	0.35	0.35
11.5	0.35	0.35
13	0.35	0.35
15	0.85	0.85
16.5	0.85	0.85
18	0.85	0.85

After cavitation tests, analysis of coated sample surfaces using electron microscope showed that at nozzle diameter 0.35 mm coating delamination is observed only at pressure increase from 10 to 13 MPa, with partial delamination in the area of maximum impact (under nozzle). External (total) diameter of cavitation mark  $D_{out}$  for nozzle diameter of 0.35 mm determined by SEM-images is bigger at distance  $H = 15$  mm (see Figure 5a,c). The increase of  $D_{out}$  is recorded with an increase in pressure.

Wear depths at distance from nozzle of 5 and 15 mm with nozzle diameter of 0.35 mm are comparable (see Figure 5c), but the greatest wear at  $H = 15$  mm is registered in annular area (see Figure 5b) located at some distance from center of cavitation mark. At  $H = 5$  mm there is wear in both the annular and central areas.

With a nozzle diameter of 0.85 mm, coating delamination is recorded in all of the tests performed. The wear depth is greater than with a nozzle diameter of 0.35 mm (see Figure 5c). At nozzle diameter 0.85 mm, with distance from nozzle of 5 and 15 mm external (total) diameters of cavitation mark  $D_{out}$  have close values. At that, for  $H = 15$  mm the delamination is more even and the delamination area is larger than for  $H = 5$  mm (see Figure 5a). The wear pattern with increase of pressure from 15 to 18 MPa does not change, the maximum wear is recorded in the center of cavitation mark (see Figure 5b). Diameter of cavitation mark  $D_{out}$  and wear depth  $h$  with pressure increase but insignificantly (see Figure 5c).

With the results of all tests carried out on coated aluminum samples, it was found that the maximum wear is at  $H = 15$  mm.

Using the mode selected on the basis of tests of coated samples, tests with blade steels 20 GL and 30 L were performed with plotting of kinetic curves of cavitation wear  $\Delta m = f(t)$ . The chemical composition of steels 20 GL and 30 L and hardness are given in Table 5. The microstructure of steels 20 GL and 30 L is shown in Figure 6.

**Table 5.** Chemical composition and hardness of steels 20 GL and 30 L.

Steel	C, %	Si, %	Mn, %	S, %	P, %	Fe, %	Hardness HB 0.1, MPa
20 GL	0.15–0.25	0.2–0.4	1.2–1.6	< 0.04	< 0.04	other	165
30 L	0.27–0.35	0.20–0.52	0.4–0.9	< 0.045	< 0.04	other	174

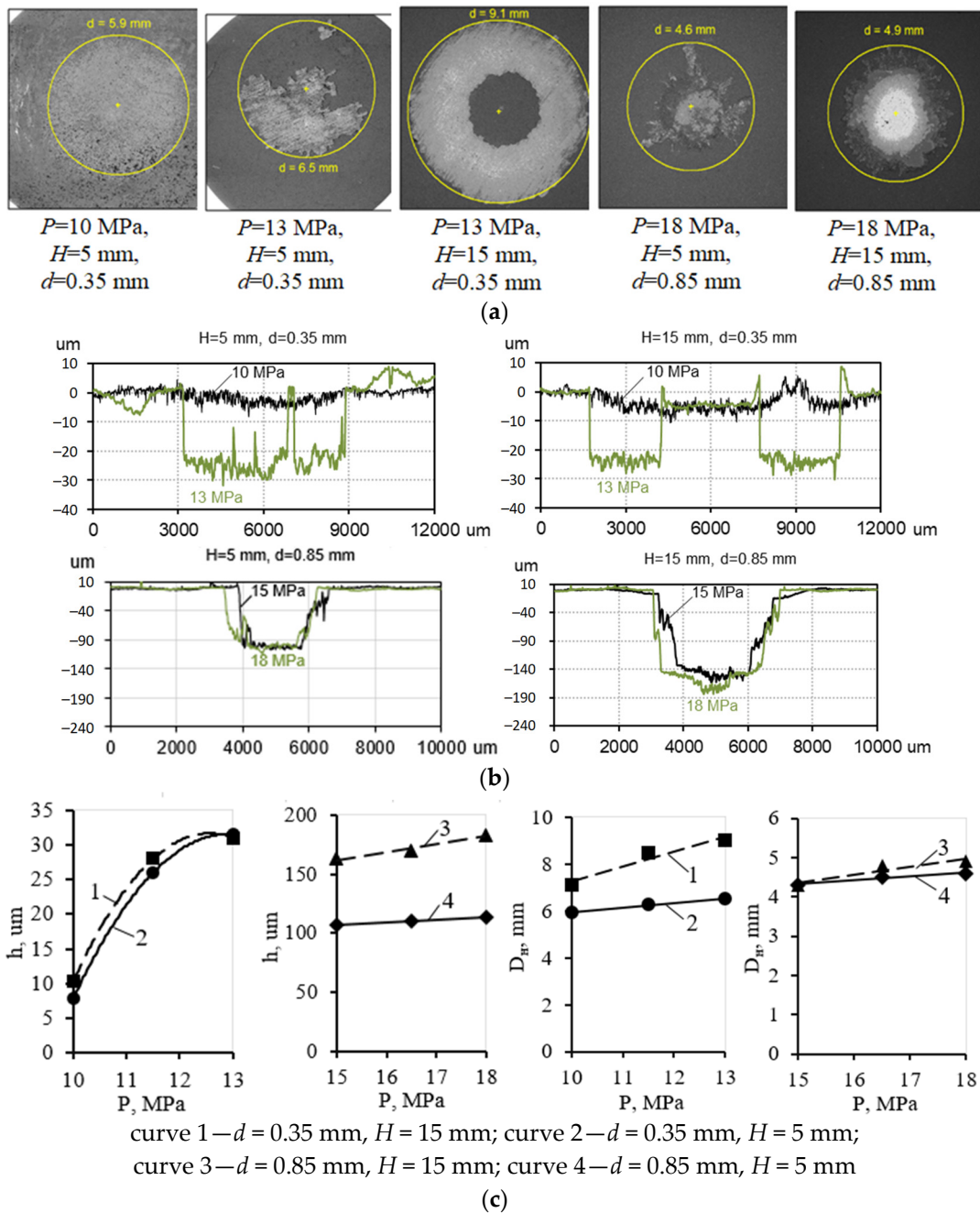


**Figure 5.** Patterns of surface changes in cavitation mark area (a), surface profiles (b), and cavitation mark depth  $h$  and cavitation mark diameter  $D_{out}$  (c) determined by them during cavitation tests of coated aluminum samples.

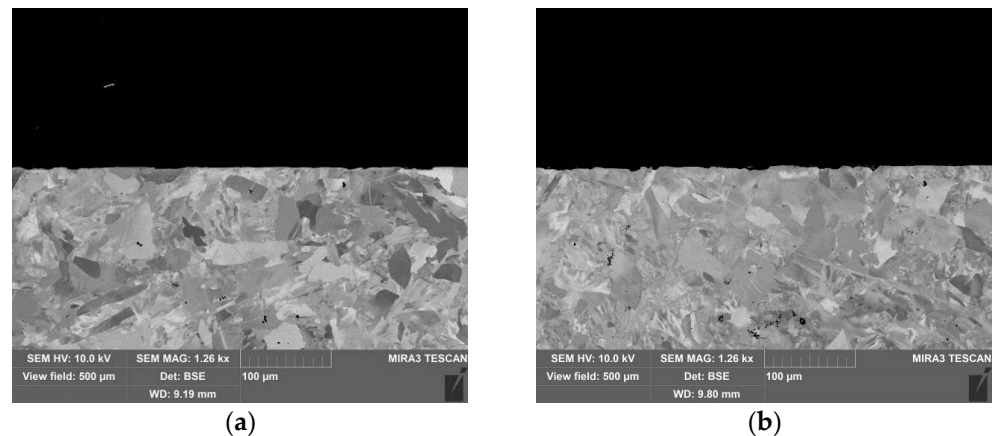


**Figure 6.** Microstructure of cast steels 20 GL (a) and 30 L (b).

For each time interval the state of sample surface was investigated with evaluation of wear depth and fracture spot sizes using mechanical stylus profiler and scanning electron microscope.

### 3. Results

Based on the results of the tests of coated aluminum samples, the following parameters were selected to ensure maximum wear in the following tests of cast steels 20 GL and 30 L: nozzle diameter of 0.85 mm, distance to nozzle of 15 mm, inlet pressure 18 MPa, outlet pressure 0.1 MPa, cavitation number 0.0055, temperature 50 °C. Cast steel samples 20 GL and 30 L were tested using these parameters. The total testing time was 210 min.

Relationships of cavitation wear of steels 20 GL and 30 L in “mass removal—testing time” plot were obtained as a result of tests (see Figure 7). The better resistance of steel 30 L to cavitation attack was found on the basis of these relationships.

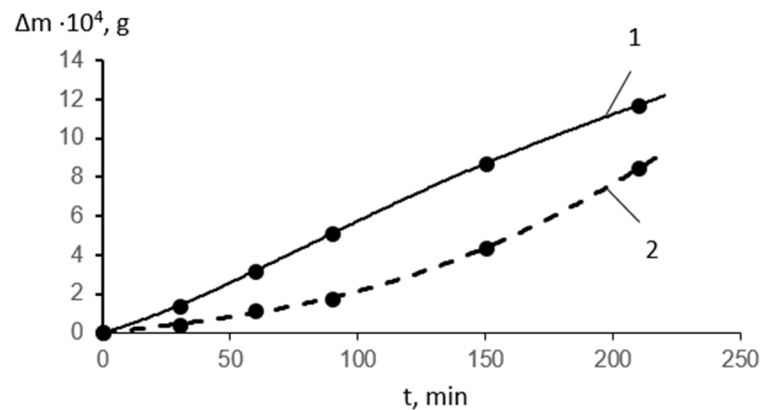


**Figure 7.** Kinetic curves of cavitation wear of steel 20 GL (1) and 30 L (2) samples.

After testing for 30, 60, 90, 150, and 210 min, the following were determined:

- Size  $D_{out}$  of the area (see Figure 8c) in which the formation and development of the cavitation pit occurs, using SEM images (see Figure 8a) of the surface;
- Wear depth  $h$  (see Figure 6d) using profiles (see Figure 8b) obtained with a surface profiler.

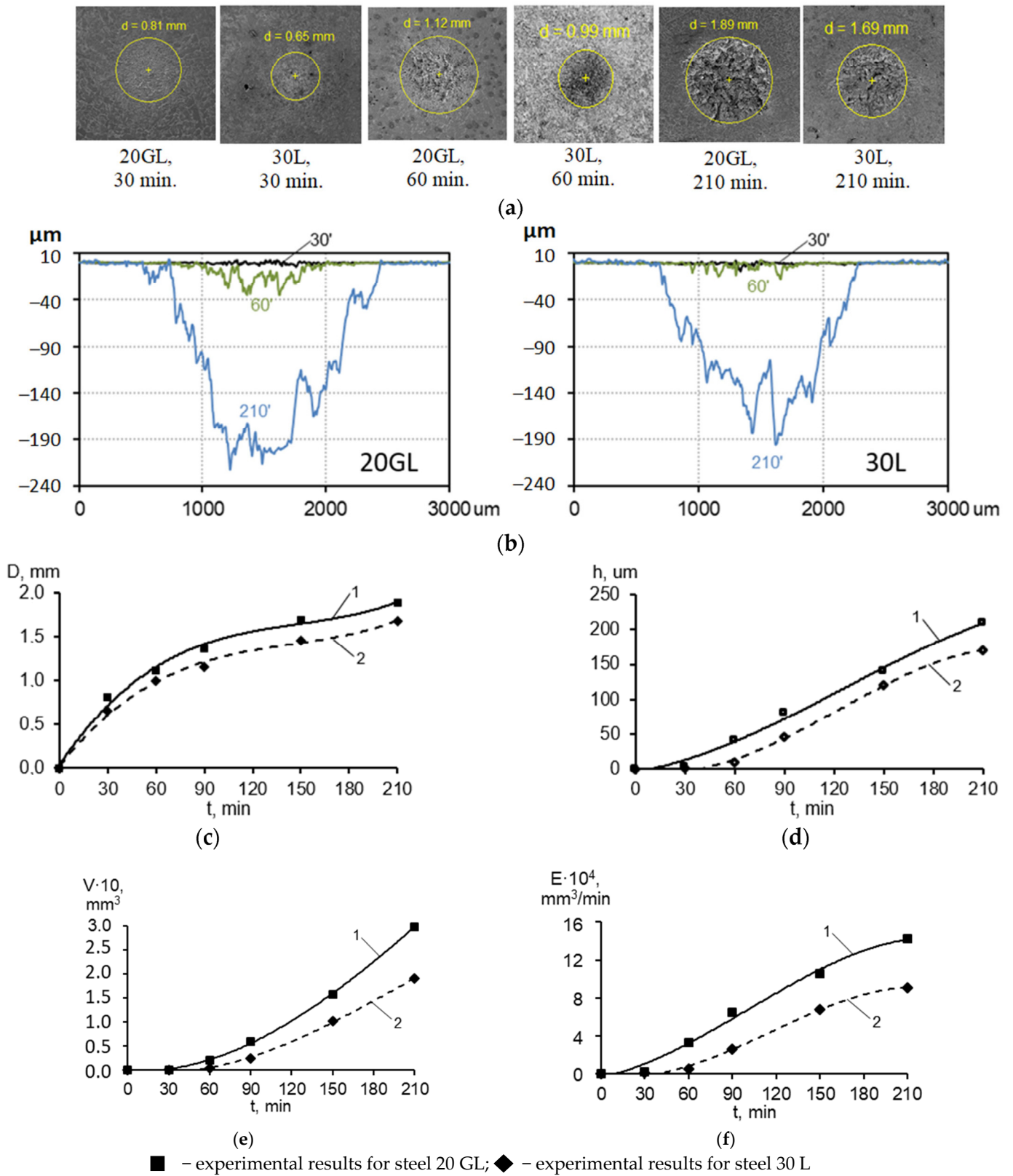


**Figure 8.** Patterns of surface changes in cavitation mark area (a), surface profiles (b), diameter of cavitation mark  $D_{out}$  (c), depth of cavitation mark  $h$  (d), volume removal  $V$  (e), and removal rate  $E$  (f) determined by them at cavitation test of steel 20 GL (1) and 30 L (2) samples (nozzle diameter 0.85 mm, distance to nozzle 15 mm, inlet pressure 18 MPa, outlet pressure 0.1 MPa, cavitation number 0.0055, temperature 50 °C).

#### 4. Discussion

The predominance of changes of cavitation mark [44–46] diameter over its depth ( $D_{out} \gg h$ ) was found during incubation period, the period with maximum rate, and the initial stage of the period with steady rate of wear of the examined cast steels. The profile shape and the ratio of  $D_{out}$  and  $h$  ( $D_{out} \gg h$ ) make it possible to evaluate the volume removal  $V$  of the sample using the formula for the ball segment (see Figure 9):

$$V = \pi h^2 \left( R - \frac{h}{3} \right) \quad (2)$$

where  $R$  is ball radius,  $h$  is the depth of cavitation mark.

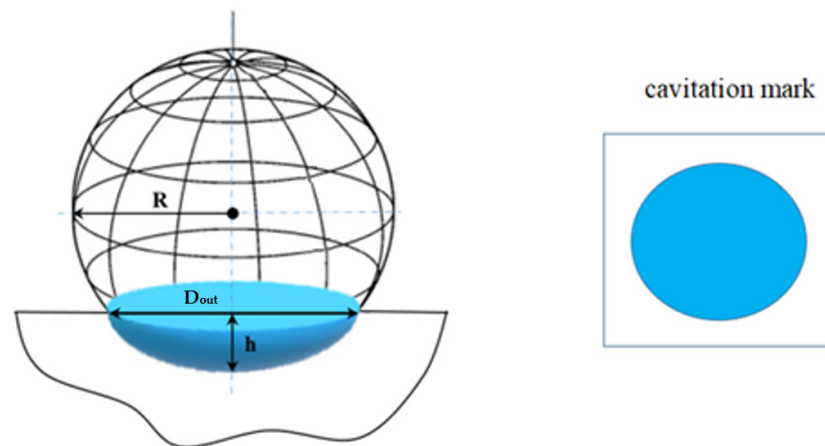


**Figure 9.** Schematic layout of diameter  $D_{out}$  and depth  $h$  of cavitation mark in ball segment shape.

The ball radius in Formula (2) is calculated using the formula:

$$R = \left( \frac{D_{out}^2}{4} + h^2 \right) / 2h \quad (3)$$

where  $D_{out}$  is diameter of cavitation mark,  $h$  is depth of cavitation mark.

Figure 8e,f show the obtained kinetic curves of volume removal and corresponding curves of volume removal rate of examined steels 20 GL and 30 L respectively.

The proposed approach for determining volume removal extends the applicability of ASTM G134-17. The determination of cavitation resistance by volume removal was previously only possible for homogeneous materials according to ASTM G134-17. Due to the application of volume removal calculation by measuring the depth and diameter of the cavitation mark, such determination can also be calculated according to formula (2) for heterogeneous materials, including after modification of their surfaces (for different types of coatings and hardenings).

In the case of an annular cavitation mark, which is also typical for cavitation jet impact [40,47], the volume removal at  $(D_{out} - D_{in}) \geq h$  can be evaluated using the formula for the torus part volume (see Figure 10):

$$V = \pi \frac{D_{in} + D_{out}}{2} \left[ R^2 \arccos \left( 1 - \frac{h}{R} \right) - \frac{1}{4} (R - h) (D_{out} - D_{in}) \right] \quad (4)$$

where  $R$  is radius of circle forming a torus during rotation,  $D_{out}$  is outer diameter of cavitation mark,  $D_{in}$  is inner diameter of cavitation mark,  $h$  is depth of cavitation mark.

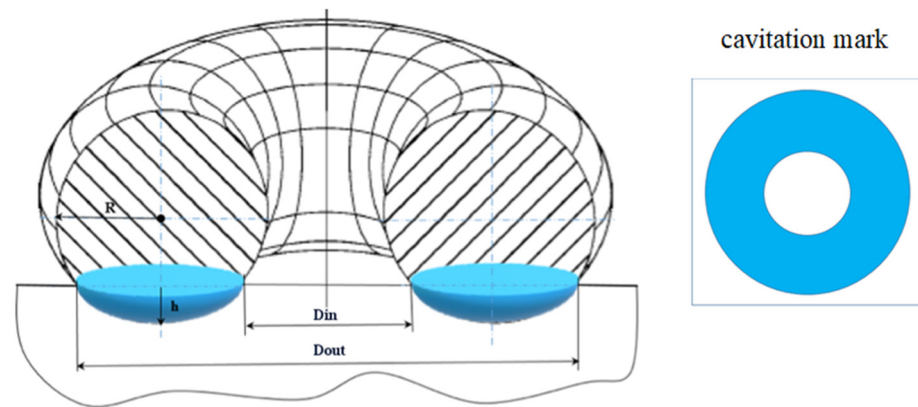


**Figure 10.** Schematic layout of diameters  $D_{out}$  and  $D_{in}$  and depth  $h$  of cavitation mark shaped as a torus segment.

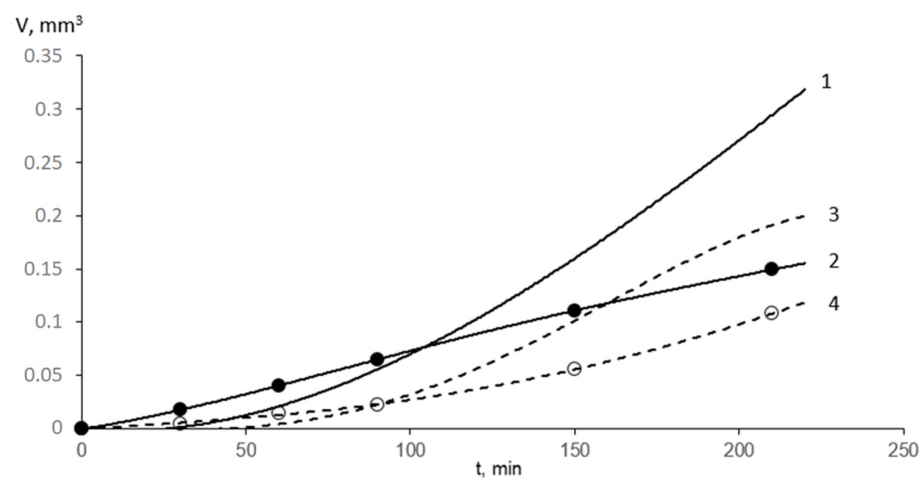
Radius of circle in Formula (4) is calculated by formula:

$$R = \left( \frac{(D_{out} - D_{in})^2}{16} + h^2 \right) / 2h \quad (5)$$

where  $D_{out}$  is diameter of cavitation mark,  $D_{in}$  is inner diameter of cavitation mark,  $h$  is depth of cavitation mark.

Discussion of the applicability of Formulas (2) and (4) requires further studies for coatings with partial material delamination in the area of maximum impact, as observed on the coated test samples.

The applicability of the Formula (2) was also assessed for estimating the volume removal of the material carried away in comparison with a well-known formula for determining volume removal using the density of a material and its measured mass removal. For the studied cast steels 20 GL and 30 L, the mass removal was determined in the framework of the experiment (see Figure 7), and the densities for these steels under normal conditions were chosen to be  $7840 \text{ kg/m}^3$  and  $7810 \text{ kg/m}^3$ , respectively. The results of comparison of calculated (without points) and experimental data (with points) for volume removal are shown in Figure 11.



● – results obtained by weight removal for steel 20 GL; ○ – results obtained by weight removal for steel 30 L

**Figure 11.** Patterns of volume removal  $V$  determined by calculation using experimentally obtained weight removal (2, 4) and by the formula for a volume removal in the form of a spherical segment using the parameters of the surface profiles (1, 3) for steels 20 GL and 30 L, respectively, during cavitation tests.

Fairly good convergence of the two considered methods for determining the volume removal revealed under cavitation exposure only in the incubation period and during the period with the maximum wear rate until 100 min of exposure. In the area with a steady wear rate up 100 min of exposure, a significant discrepancy was recorded in the data obtained on the volume removal, obtained by processing the profile of their surface (curves 1, 3) and determined by the weight removal (curves 2, 4). This circumstance, apparently, is caused by the fact that when formula (2) is used, it does not take into account the significantly changed relief of the damaged surface, as a result of which the obtained volume loss value is overestimated (see Figure 12), what can be the reserve coefficient when calculating the cavitation resistance of materials and methods of their protection according to the proposed formula.



**Figure 12.** Schematic depiction of the capturing by a spherical segment of the calculated volume removal of material in comparison with the real volume removal of a complex figure bounded by a complex surface profile, calculated using an experimentally determined mass removal.

## 5. Conclusions

As a result of cavitation tests according to ASTM G134-17, the wear kinetic of cast steels 20 GL and 30 L was determined under the selected parameters of maximum cavitation jet impact. It showed that 30 L steel has better cavitation resistance.

The analysis of the examined cast steel surface changes in time by profilometry and microscopy techniques confirmed the predominance of cavitation mark diameter over its depth during the incubation period and the period with maximum wear rate. A formula for calculating volume material removal has been proposed based on the data obtained.

As a result of this study, an improved approach to evaluation of volume material removal according to ASTM G134-17 is proposed, which is calculated using typical dimensions of cavitation mark. This approach allows to calculate volume removal at incubation period and the period with maximum wear rate not only for homogeneous, but also for heterogeneous materials, which can be various types of diffusion and metallic coatings. The use of such an approach can significantly extend the applicability limitations of ASTM G134-17.

**Author Contributions:** Conceptualization, A.M., O.Z. and A.T.; methodology, O.Z.; experiment, A.M. and A.T.; validation, M.D. and A.M.; formal analysis, O.Z. and M.D.; investigation, A.M.; data curation, O.Z. and A.M.; writing—original draft preparation, O.Z., M.D. and A.M.; writing—review and editing, A.T.; visualization, M.D. and A.M.; supervision, S.G.; project administration, A.M. and O.Z.; funding acquisition, S.G., O.Z. and A.M. All authors have read and agreed to the published version of the manuscript.

**Funding:** The study was conducted in the framework of a proactive research on “Study to improve the thermal-hydraulic properties and wear resistance of functional surfaces of power equipment”.

**Institutional Review Board Statement:** Not applicable.

**Informed Consent Statement:** Not applicable.

**Data Availability Statement:** Not applicable.

**Conflicts of Interest:** The authors declare no conflict of interest.

## References

1. Pris, C. *Erosion: English Translation*, 1st ed.; Mir: Moscow, Russia, 1982; pp. 100–150.
2. Pylaev, N.I.; Edel, J.U. *Cavitation in Water Turbines*, 1st ed.; Mashinostroenie: Saint Petersburg, Russia, 1974; pp. 84–95.

3. Brijkishore; Khare, R.; Prasad, V. Prediction of cavitation and its mitigation techniques in hydraulic turbines—A review. *Ocean Eng.* **2021**, *221*, 108512. [[CrossRef](#)]
4. Rodionov, V.P.; Ukolov, A.I. The laws of cavitation erosion of construction materials. *Her. Dagestan State Tech. Univ. Tech. Sci.* **2017**, *44*, 39–47. [[CrossRef](#)]
5. Tarasov, V.N. Physics of cavitation damage. *Electron. J. Tech. Acoust.* **2015**, *3*. Available online: <https://ejta.org/en/tarasov1> (accessed on 16 December 2022).
6. Rao, N.S.G.; Thiruvengadam, A. Prediction of cavitation damage. *Trans. Am. Soc. Civ. Eng.* **1962**, *127*, 309–334. [[CrossRef](#)]
7. Thiruvengadam, A. A Unified theory of cavitation damage. *J. Fluids Eng.* **1963**, *85*, 365–373. [[CrossRef](#)]
8. Tichler, J.W.; Elsen, J.B.v.d.; Gee, A.W.J.d. Resistance against cavitation erosion of 14 chromium steels. *J. Tribol.* **1970**, *92*, 220–226. [[CrossRef](#)]
9. Hattori, S.; Ishikura, R. Revision of cavitation erosion database and analysis of stainless steel data. *Wear* **2010**, *268*, 109–116. [[CrossRef](#)]
10. Karimi, W.R.L. Phenomenological model for cavitation erosion rate computation. *Mater. Sci. Eng.* **1987**, *95*, 1–14. [[CrossRef](#)]
11. Berchiche, N.; Franc, J.P.; Michel, J.M. A cavitation erosion model for ductile materials. *J. Fluids Eng.* **2002**, *124*, 601–606. [[CrossRef](#)]
12. Hattori, S.; Maeda, K. Logistic curve model of cavitation erosion progress in metallic materials. *Wear* **2010**, *268*, 855–862. [[CrossRef](#)]
13. Plessset, M.S.; Ellis, A.T. On the mechanism of cavitation damage. *Trans. ASME* **1955**, *77*, 1055–1064. [[CrossRef](#)]
14. Jahangir, S.; Ghahramani, E.; Neuhauser, M.; Bourgeois, S.; Benschow, R.E.; Poelma, C. Experimental investigation of cavitation-induced erosion around a surface-mounted bluff body. *Wear* **2021**, *480–481*, 203917. [[CrossRef](#)]
15. Shi, Y.; Luo, K.; Chen, X.; Li, D.; Jia, L. A new cavitation model considering inter-bubble action. *Int. J. Nav. Arch. Ocean Eng.* **2021**, *13*, 566–574. [[CrossRef](#)]
16. Sagar, H.J.; Moctar, O.e. Dynamics of a cavitation bubble near a solid surface and the induced damage. *J. Fluids Struct.* **2020**, *92*, 102799. [[CrossRef](#)]
17. Xu, W.-L.; Li, J.-B.; Luo, J.; Zhai, Y.-W. Effect of a single air bubble on the collapse direction and collapse noise of a cavitation bubble. *Exp. Therm. Fluid Sci.* **2021**, *120*, 110218. [[CrossRef](#)]
18. Krella, A.; Tekumalla, S.; Gupta, M. Influence of micro Ti particles on resistance to cavitation erosion of Mg-xTi composites. *Mech. Mater.* **2021**, *154*, 103705. [[CrossRef](#)]
19. Peng, C.; Tian, S.; Li, G.; Wei, M. Enhancement of cavitation intensity and erosion ability of submerged cavitation jet by adding micro-particles. *Ocean Eng.* **2020**, *209*, 107516. [[CrossRef](#)]
20. Vuksanović, M.M.; Gajić-Kvaščev, M.; Husović, T.V.; Heinemann, R.J. Advanced damage resistance monitoring procedure on the composite materials' surface-exposed to cavitation testing. *Wear* **2021**, *474–475*, 203877. [[CrossRef](#)]
21. Santos, L.L.; Cardoso, R.P.; Brunatto, S.F. Behavior of the reversed austenite in CA-6NM martensitic stainless steel under cavitation. *Wear* **2020**, *454–455*, 203322. [[CrossRef](#)]
22. Khvatov, B.N. Influence of surface layer condition on cavitation erosion kinetics of water turbine steel. *Vestnik TSTU* **2002**, *8*, 507–512.
23. Usta, O.; Koksall, C.S.; Korkut, E. A Study on Cavitation Erosion Resistance of Marine Propeller Materials, Using a Water Jet Test Rig. In Proceedings of the Colloquium Series 3rd International Meeting—Progress in Propeller Cavitation and Its Consequences: Experimental and Computational Methods for Predictions, Istanbul, Turkey, 15–16 November 2018; pp. 1–10.
24. Linderov, M.L.; Merson, D.L. Effect of cavitation on surface degradation of structural steels. *Vector Nauki TSU.* **2010**, *3*, 43–45.
25. Shi, Z.; Wang, J.; Wang, Z.; Qiao, Y.; Xiong, T.; Zheng, Y. Cavitation Erosion and Jet Impingement Erosion Behavior of the NiTi Coating Produced by Air Plasma Spraying. *Coatings* **2018**, *8*, 346. [[CrossRef](#)]
26. Krella, A.K. Cavitation erosion of monolayer PVD coatings—An influence of deposition technique on the degradation process. *Wear* **2021**, *478–479*, 203762. [[CrossRef](#)]
27. Petrov, A.I.; Skobelev, M.M.; Khanychev, A.G. Study of comparative resistance to cavitation erosion of materials samples and coatings in the hydraulic machine flow sections. *Her. Bauman Mosc. = State Tech. University. Ser. Mech. Eng.* **2015**, *2*, 128–137.
28. Zubrilov, S.P.; Rastrigin, N.V. Studying the cavitation process and the possibility of reducing erosive wear. *Vestn. Gos. Univ. Morskogo I Rechn. Flot. Im. Admirala SO Makarova* **2019**, *11*, 705–717. [[CrossRef](#)]
29. Thiruvengadam, A.; Waring, S. Mechanical properties of metals and their cavitation-damage resistance. *J. Ship Res.* **1966**, *10*, 1–9. [[CrossRef](#)]
30. Steller, J.; Krella, A.; Koronowicz, J.; Janicki, W. Towards quantitative assessment of material resistance to cavitation erosion. *Wear* **2005**, *258*, 604–613. [[CrossRef](#)]
31. Sreedhar, B.K.; Albert, S.K.; Pandit, A.B. Cavitation damage: Theory and measurements—A review. *Wear* **2017**, *372–373*, 177–196. [[CrossRef](#)]
32. Cai, T.; Pan, Y.; Ma, F. Effects of nozzle lip geometry on the cavitation erosion characteristics of self-excited cavitating waterjet. *Exp. Therm. Fluid Sci.* **2020**, *117*, 110137. [[CrossRef](#)]
33. Hong, S.; Wu, Y.; Wu, J.; Zheng, Y.; Zhang, Y.; Cheng, J.; Li, J.; Lin, J. Effect of flow velocity on cavitation erosion behaviour of HVOF sprayed WC10Ni and WC-20Cr3C2-7Ni coatings. *Int. J. Refract. Met. Hard Mater.* **2020**, *92*, 105330. [[CrossRef](#)]
34. Schreiner, F.; Hanke, S.; Skoda, R. Assessment of flow aggressiveness and erosion damage topography for different gap widths in ultrasonic cavitation testing. *Wear* **2021**, *484–485*, 203989. [[CrossRef](#)]

35. Fujisawa, N.; Horiuchi, T.; Fujisawa, K.; Yamagata, T. Experimental observation of the erosion pattern, pits, and shockwave formation in a cavitating jet. *Wear* **2019**, *418–419*, 265–272. [[CrossRef](#)]
36. Bansal, A.; Singh, J.; Singh, H.; Goyal, D.K. Influence of thickness of hydrophobic polytetrafluoroethylene (PTFE) coatings on cavitation erosion of hydro-machinery steel SS410. *Wear* **2021**, *477*, 203886. [[CrossRef](#)]
37. Teran, L.A.; Laín, S.; Rodríguez, S.A. Energy effect modelling of cavitation and hard particle erosion: Implementation and validation. *Wear* **2021**, *478–479*, 203901. [[CrossRef](#)]
38. Pandey, S.; Bansal, A.; Omer, A.; Singla, A.K.; Goyal, D.K.; Singh, J.; Gupta, M.K. Effect of fuel pressure, feed rate, and spray distance on cavitation erosion of Rodojet sprayed Al<sub>2</sub>O<sub>3</sub>+50%TiO<sub>2</sub> coated AISI410 steel. *Surf. Coat. Technol.* **2021**, *410*, 126961. [[CrossRef](#)]
39. Kang, C.; Liu, H.; Soyama, H. Estimation of aggressive intensity of a cavitating jet with multiple experimental methods. *Wear* **2018**, *394–395*, 176–186. [[CrossRef](#)]
40. Pan, Y.; Ma, F.; Liu, B.; Cai, T. Cavitation intensity and erosion pattern of a self-excited cavitating jet. *J. Mater. Process. Technol.* **2020**, *282*, 116668. [[CrossRef](#)]
41. Liu, Y.; Wu, Q.; Huang, B.; Zhang, H.; Liang, W.; Wang, G. Decomposition of unsteady sheet/cloud cavitation dynamics in fluid-structure interaction via POD and DMD methods. *Int. J. Multiph. Flow* **2021**, *142*, 103690. [[CrossRef](#)]
42. Fujisawa, N.; Fujita, Y.; Yanagisawa, K.; Fujisawa, K.; Yamagata, T. Simultaneous observation of cavitation collapse and shock wave formation in cavitating jet. *Exp. Therm. Fluid Sci.* **2018**, *94*, 159–167. [[CrossRef](#)]
43. *ASTM G134-17*; Standard Test Method for Erosion of Solid Materials by a Cavitating Liquid Jet. ASTM INTERNATIONAL: West Conshohocken, PA, USA, 2017.
44. Hutli, E.; Nedeljkovic, M.S.; Radovic, N.A.; Bonyár, A. The relation between the high speed submerged cavitating jet behaviour and the cavitation erosion process. *Int. J. Multiph. Flow* **2016**, *83*, 27–38. [[CrossRef](#)]
45. Sasaki, H.; Takeo, F.; Soyama, H. Cavitation erosion resistance of the titanium alloy Ti–6Al–4V manufactured through additive manufacturing with various peening methods. *Wear* **2020**, *462–463*, 203518. [[CrossRef](#)]
46. Liu, B.; Ma, F. Erosion behavior of aluminum by an inclined cavitating jet. *Wear* **2021**, *474–475*, 203751. [[CrossRef](#)]
47. Hutli, E.; Nedeljkovic, M.; Bonyár, A. Cavitating flow characteristics, cavity potential and kinetic energy, void fraction and geometrical parameters—Analytical and theoretical study validated by experimental investigations. *Int. J. Heat Mass Transf.* **2018**, *117*, 873–886. [[CrossRef](#)]

**Disclaimer/Publisher’s Note:** The statements, opinions and data contained in all publications are solely those of the individual author(s) and contributor(s) and not of MDPI and/or the editor(s). MDPI and/or the editor(s) disclaim responsibility for any injury to people or property resulting from any ideas, methods, instructions or products referred to in the content.